The development of filter vector magnetographs for the Solar Magnetic Activity Research Telescope (SMART)

S. UeNo*[a], S. Nagata[a], R. Kitai[a], H. Kurokawa[a], K. Ichimoto[b], SMART-developing team[a]
[a]Kwasan & Hida Observatories, Kyoto Univ./ Kurabashira, Kamitakara, Yoshiki-gun, Gifu 506-1314, JAPAN;
[b]National Astronomical Observatory of Japan, 2-21-1 Ohsawa, Mitaka, Tokyo 181-8588, JAPAN

ABSTRACT

In recent years, it is beginning to be shown observationally and theoretically that the existence of the magnetic field is indispensable for active phenomena on the solar surface. In particular, the rotation or helicity of the magnetic field and their temporal variation are considered to be important factors which influence solar activity. In order to confirm this, it is necessary to compute vector components of the magnetic field with a higher accuracy than before. Therefore, we developed two kinds of filter-type magnetographs for the Solar Magnetic Activity Research Telescope (SMART) at Hida observatory, which allow us to observe the polarization components in sunlight with high accuracy. We use a Lyot filter in one of two sets of magnetographs. On the other hand, a tandem-typed Fabry-Perot filter is used in one more set. For these two instruments, we made the following concrete advances.

1. The method of coating of the pre-filters.
2. Special fine-anneal on the main lenses.
3. Highly accurate rotating wave-plate.
4. Simultaneous observation of two kinds of filtergrams which have orthogonally polarized light mutually by using Fabry-Perot channel.
5. Observation in four wavelengths which can suppress various errors.
6. Low apparent Doppler shift in the FOV due to the oblique incidence of the rays to the filters.
7. Large format CCD (large-sized chip, large full-well).
8. High speed data transfer interface between the CCD and PC.

In this paper, we report the details of these points, the expected effect of them, and the results of initial measurements.

Keywords: magnetograph, Lyot, Fabry-Perot, Stokes, polarimeter, magnetic field, polarization

1. INTRODUCTION

We built a new telescope named the Solar Magnetic Activity Research Telescope (SMART) at Hida observatory from 2002 through 2003. The SMART has two purposes, the 1st one is “the observation of all active phenomena on the full solar disk with high spatial and temporal resolution”, the 2nd one is “the measurement of vector magnetic fields on the full solar disk with high spatial resolution and high accuracy”. By realizing these purposes, we intend to study various subjects, such as

- Studies of the emerging process of twisted magnetic flux tubes, which are essential for the occurrence of strong solar flares.
- Investigations of the detailed structures of magnetic flux tubes and features and the processes through which they accumulate and release energy.
- Studies of the distribution and the time-variation of the magnetic field’s helicity around active regions.
- Investigation of the vector magnetic field and its evolution at the foot-points of hot and cool quasi-steady coronal loops.
- Studies of the relationship between the photospheric gas motion and the variation of magnetic configurations.

We have developed two sets of magnetographs, in order to realize the above-mentioned 2nd purpose especially.
In recent years, the accumulation of digitalized data from various magnetographs and the development of MHD simulations have progressed, and it is beginning to be shown observationally and theoretically that the existence of the magnetic field is indispensable for active phenomena on the solar surface. In particular, the rotation or helicity of the magnetic field and their temporal variations are considered to be important factors which influence solar activity (for

*ueno@kwasan.kyoto-u.ac.jp; phone +81-578-6-2311; fax +81-578-6-2118

Ground-based Instrumentation for Astronomy, edited by
Alan F.M. Moorwood, Masanori Iye, Proceedings of SPIE Vol. 5492
(SPIE, Bellingham, WA, 2004). 0277-786X/04/$15. doi: 10.1117/12.550304

example, K. Kusano et al. 2002). However, observational studies, which can directly confirm that the change of some index corresponds to the occurrence of the solar flare, have not been performed yet because of restrictions in the observation accuracy. In order to confirm our theories, it is necessary to compute vector components of the magnetic field with higher accuracy than before. In general, this subject is, however, very difficult because of the technical restrictions of optical elements and detectors in telescopes or polarimeters.
Therefore, in the process of developing our two kinds of filter-type magnetographs, we have performed various improvements from various sides, so that we can observe the polarization components in sunlight with high accuracy.

1. STRUCTURES OF THE TELESCOPES IN WHICH THE MAGNETOGRAPHS ARE INSTALLED

The SMART is installed on a platform whose height including a steel tower and a foundation is 16m from the ground (fig.1). It consists of four refractors, which we call T1, T2, T3 and T4 respectively.
T1 has a refractive lens with 20 cmϕ aperture and a Lyot filter, and obtains full solar disk images in the wavelength range H$\alpha \pm 2$ Å. T2 is the magnetograph. It has a refractive lens with 20 cmϕ aperture, a polarimeter including a rotating wave-plate and a polarizer, and a Lyot filter. It obtains two kinds of magnetograms in full-disk mode or in partial-region mode by exchanging two sets of collimator lens units and imaging lens units. T3 has a refractive lens with 25 cmϕ aperture and a large Lyot filter, and obtains partial-region images with higher spatial resolution than T1 in the wavelength range H$\alpha \pm 2$ Å. T4 is a multi-channel telescope which has a refractive lens with 25 cmϕ aperture. By exchanging optical elements between a telecentric lens and a CCD camera of T4, we can select two kinds of observation modes; one is a 2 color imager mode and the other is the magnetograph mode. The former is used for obtaining photospheric images and chromospheric images by Fabry-Perot filters. The latter is used for obtaining two simultaneous images of orthogonally polarized light of the partial photosphere with higher spatial resolution than T2 using a Fabry-Perot filter.
The main characteristics of the two telescopes (T2, T4) in which the magnetographs are installed are shown in table 1. Their interior structures are also shown in fig.2. These telescopes have a pair of wedge-shaped pre-filters at the head. The purpose of these pre-filters is that we can select any positions on the sun by rotating these two glass plates, even if the telescope itself points to the center of the solar disk.

Fig. 1. The exterior of the SMART

Table 1. Characteristics of the two telescopes in which the magnetographs are installed

Telescope Name	Aperture [cm]	Observed Image, Wavelength & passband	FOV [arcsec]	The Number of CCD pixel	Pixel Resolution [arcsec/pixel]	Spatial Resolution [arcsec]
T2	20	Vector magnetogram, 6302.5Å, $\Delta\lambda$: 0.125Å (Full-disk mode)	2000x2000	2000x2000	1.0	1.58
		6302.5Å, $\Delta\lambda$: 0.125Å (Partial-region mode)	500x500	2000x2000	0.25	0.79
T4	25	Vector magnetogram (2 kinds of polarized images) 6302.5Å, $\Delta\lambda$: 0.101Å	400x400	4000x4000	0.10	0.63
		(Partial region with higher spatial resolution)	400x400	4000x4000	0.10	0.63

1. TARGET SPECIFICATIONS OF THE MAGNETOGRAPHS

When we began to develop magnetographs in SMART, we established the following target specifications for the photometric accuracy for the Stokes parameters and the temporal resolution for one series of data.

Target of the photometric accuracy

We use this term "photometric accuracy" to mean the measurement error of each Stokes parameter at a certain wavelength. This term includes all measurement errors, such as the photon-shot noise due to the CCD chip, the cross-talk between Stokes parameters due to optical elements, the indefinite photometric error due to non-uniformity of the filter transmission profile, and so on.

Though it is better that these errors are smaller, at this time, we set the target of the photometric accuracy as follows;

$$(\text{photometric accuracy}) \leqq 0.1\% \qquad (1).$$

Then, finally, we would like to measure the strength of the vector magnetic field with an accuracy within 10 % of the error for any strength of the magnetic field. As a result of a simulation of the sensitivity of the Stokes profiles, which were calculated from the LTE model atmosphere of Holweger & Muller (1974), to the magnetic field strength, the value

Fig. 2. Interior structures of two telescopes in which magnetographs are installed.

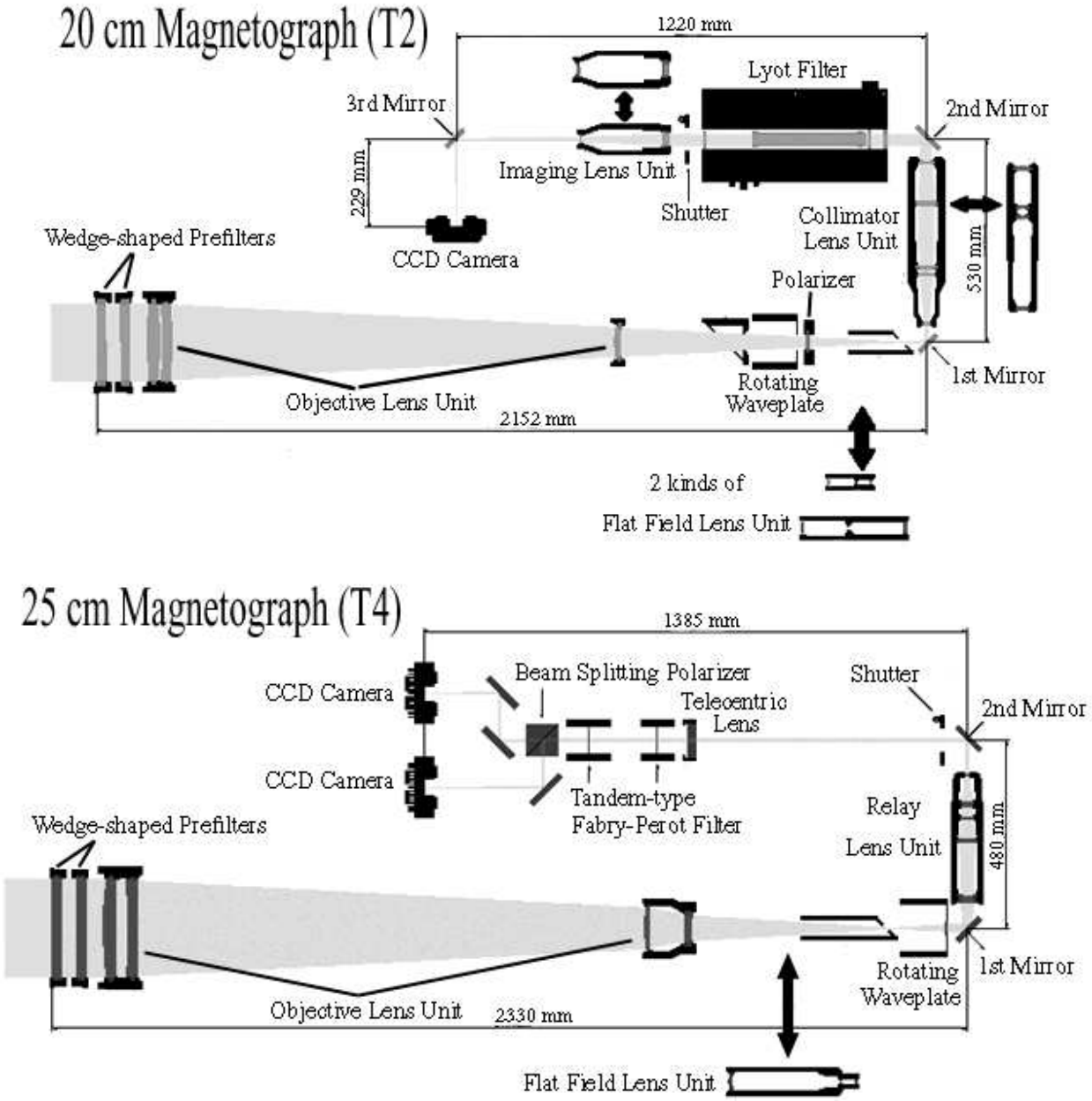

of $\pm 0.1\%$ of the error corresponds to $\Delta B_l < \pm 6$ - 7 G for the longitudinal magnetic field, and $\Delta B_t < \pm 15 - 50$ G for the transversal magnetic field (when B_l, $B_t \leqq 500$ G).

Target of the temporal resolution (the observation cadence)

One series of data of our SMART magnetograph consists of 16 frames (four angles of the wave-plate at four wavelengths in an absorption line) in the case of the T2-magnetograph or 12 frames (three angles of the wave-plate at four wavelengths in a absorption line) in the case of the T4-magnetograph. We set the target of the temporal resolution (the observation cadence) for every series as follows;

$$\text{(temporal resolution)} \leqq 30 \text{ sec} \qquad (2).$$

First of all, this value is connected with the velocity of the structures to be observed, which move on the solar photosphere. If we consider that a structure which moves only within a half distance of the pixel-resolution for 30 sec has not moved, the velocity of a moving structure which can be coped with our magnetograph is $\leqq$12 km/s for the full-disk mode of T2, $\leqq$3.0 km/s for the partial-region mode of T2 and $\leqq$1.2 km/s for T4, respectively. Therefore, for example, we can observe the magnetic field at foot-points of moving magnetic loops in an emerging flux region with low error using the T2-magnetograph, and we can observe the magnetic field of small-sized magnetic structures which drift on the flow of super-granulations with low error using the T4-magnetograph.

Secondly, this target value is related with the strength of the negative influence of photospheric 5-min oscillations on the photometric accuracy. Since the typical size of change of the Doppler velocity due to 5-min oscillations is about 1 km/s for 150 sec, it is considered that the change for 30 sec (=$\pm$15 sec) is about 0.2 km/s (=$\pm$0.1 km/s). According to the results of our simulation of the Stokes profiles using the above-mentioned model atmosphere, this value of change of the Doppler velocity, which corresponds to a wavelength shift of 2 mÅ, gives a photometric error of 0.1 % at $\pm$0.07 Å from the line-center. Therefore, we want to suppress the temporal resolution within 30 sec also in order to realize the above-mentioned target for the photometric accuracy.

4. DEVISED POINTS IN DEVELOPING HIGHLY ACCURATE MAGNETOGRAPHS

The target specifications mentioned in section 3 are not easy to achieve because of the technical restrictions of the optical elements and detectors in telescopes or polarimeters, but we made the following improvements on various sides in order to make the actual specifications as close to the targets as possible.

1. Coating on wedge-shaped pre-filters (for suppressing the instrumental polarization)
2. Anneal of glass materials for pre-filters and lenses (for suppressing the instrumental polarization)
3. High quality rotating wave-plate (for suppressing the error of the polarimeter itself)
1. Simultaneous recording two images of orthogonally polarized light using Fabry-Perot channel (for suppressing the error of the polarimeter and the influence of the seeing conditions)
5. Observation of four wavelengths in an absorption line (for suppressing the photon-shot noise of the CCD, the influence of non-uniformity of the filters, the error of the inversion method, and so on)
6. A wavelength shift in the FOV due to the oblique incidence of the rays to the filters (for suppressing the error of the inversion method)
7. Large format and highly sensitive CCD cameras (for suppressing the photon-shot noise of the CCD)
8. A high speed data transfer interface from the CCD to the PC (for improving the temporal resolution)

In this section, we introduce each of these points in detail.

4.1 Coating on wedge-shaped pre-filters

When the vacuum evaporation of the filter-coating is carried out only from one direction to a glass surface with a normal evaporator, coated particles are arranged with a certain directivity at each point (fig.3(a)). As a result, the filter shows the behavior of retarders and it can modulate the incident Stokes parameters. Here, we assume that the coated filter has the same Muller matrix as linear retarders, and the maximum value of the circular-polarization component (V) in the sunlight is 0.3. Then the maximum cross-talk from V to the linear-polarization components (Q, U) exceeds 0.1 % of the incident intensity (I), when the retardation of a coated filter exceeds 0.33 nm.

Therefore, we set the following specification, when we produced the wedge-shaped pre-filters of T2 and T4.

$$\text{(Total retardation of each coated-filter)} \leqq 0.3 \text{ nm} \qquad (3).$$

For example, when the coated filter has a retardation of $\pm$0.3 nm, the error due to this filter for the incident Stokes parameters is expressed by the following matrix;

$$\Delta\begin{pmatrix} I \\ Q \\ U \\ V \end{pmatrix} = \begin{pmatrix} 0 & 0 & 0 & 0 \\ 0 & \mp 4\times10^{-6}\sin^2 2\theta & \pm 4\times10^{-6}\sin 2\theta\cos 2\theta & \mp 0.003\sin 2\theta \\ 0 & \pm 4\times10^{-6}\sin 2\theta\cos 2\theta & \mp 4\times10^{-6}\cos^2 2\theta & \pm 0.003\cos 2\theta \\ 0 & \pm 0.003\sin 2\theta & \mp 0.003\cos 2\theta & \mp 4\times10^{-6} \end{pmatrix}\begin{pmatrix} I \\ Q \\ U \\ V \end{pmatrix} \quad (4)$$

where θ is the angle of the retarder's fast-axis.

Therefore, we suggested using a "planetary rotating vacuum evaporation system (fig. 3(b))" for coating to the coating maker in order to suppress the retardation. As a result of the measurement of the retardation at only one point on the sample filter which was made with the same system, the retardation value was 1.502 nm. However, the total retardation of each pre-filter must be much smaller, because rays which are focused to one point on the focal plane pass through the whole filter surface and the total retardation is an average of retardations which have different axis-angles (θ) at every point on the filter surface. Though we have not measured the retardation of the actual pre-filters in a laboratory, we intend to perform the measurement of the total retardations or Muller matrices of them by entering several kinds of known polarized light into telescopes, where pre-filters are actually attached at the head of the telescopes.

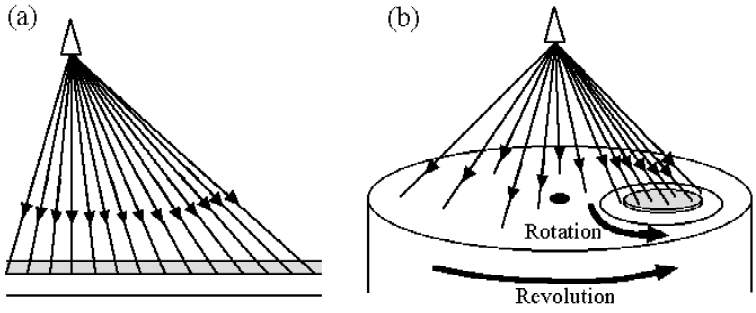

Fig. 3. (a) Normal vacuum evaporator, (b) Planetary rotating vacuum evaporation system

4.2 Anneal of glass materials for pre-filters and lenses

In general, strains due to stress which occur in the annealing process of glass materials generate birefringence inside the glass. Therefore, strictly speaking, we can consider that the normal glass is the aggregate of various linear retarders which have different retardations and different axis-angles. In the two kinds of magnetograph of the SMART, the following glass elements are installed between the entrance and the polarimeter (a wave-plate and a polarizer).

- T2-magnetograph: wedge-shaped pre-filters (2 plates), objectives (3 pieces)
- T4-magnetograph: wedge-shaped pre-filters (2 plates), objectives (4 pieces) relay lens unit (7 pieces), telecentric lens (1piece), beam splitting polarizer (1 piece)

If the remaining strains of these glass elements are large, the Stokes parameters of the incident light into the polarimeter are changed by those elements and have significantly different values from the ones of the original sunlight. Therefore, we set up the following target specification for the same reason as the above-mentioned specification about the coating to the pre-filters.

(Total retardation due to remaining strains of each element) $\leqq$ 0.33 nm ($0.33/d_g$ nm/cm) (5),

where d_g is the thickness (unit: cm) of each glass element.

However, we knew that the typical retardation due to the remaining strains of the normally annealed glass is generally very large; about 5 nm/cm. Therefore, we performed the "fine-anneal" for all glass materials of the above elements. In the fine-anneal process, we repeated the circulation process of melting and cooling of glass materials twice, and we spent 2 – 3 times as much time as the normal process on cooling of the materials. As a result, we could make highly uniform glass materials whose retardation is much smaller than that of normal products. When we measured the retardations at 25 points on each glass material in a laboratory, the averaged absolute values were 0.300 – 1.12 nm/cm. Though these values exceed the specified value in (5), they stand for each averaged retardation at a certain point on each piece of material. So, the total retardation of each glass element must be much smaller, because rays which are focused to one point on the focal plane pass through the whole glass element and the total retardation is averaged. We will also measure the total retardations or Muller matrices of these glass elements by entering several kinds of known polarized lights into actual telescopes.

4.3 High quality rotating wave-plate

Both polarimeters in the SMART-magnetographs include one linear retarder and one polarizer.

The relation between the two Stokes vectors of the light before passing through the polarimeter and of the light after

passing through the polarimeter is ideally expressed with the following formulae.

$$\mathbf{S_{out}} = \mathbf{P}\,\mathbf{W}\,\mathbf{S_{in}} \tag{6}$$

$$\begin{pmatrix} I_{out} \\ Q_{out} \\ U_{out} \\ V_{out} \end{pmatrix} = \frac{1}{2} \begin{pmatrix} 1 & 1 & 0 & 0 \\ 1 & 1 & 0 & 0 \\ 0 & 0 & 0 & 0 \\ 0 & 0 & 0 & 0 \end{pmatrix} \begin{pmatrix} 1 & 0 & 0 & 0 \\ 0 & 1-(1-\cos\delta_W)\sin^2 2\theta_W & (1-\cos\delta_W)\sin 2\theta_W \cos 2\theta_W & \sin\delta_W \sin 2\theta_W \\ 0 & (1-\cos\delta_W)\sin 2\theta_W \cos 2\theta_W & (1-\cos\delta_W)\cos^2 2\theta_W & -\sin\delta_W \cos 2\theta_W \\ 0 & -\sin\delta_W \sin 2\theta_W & \sin\delta_W \cos 2\theta_W & \cos\delta_W \end{pmatrix} \begin{pmatrix} I_{in} \\ Q_{in} \\ U_{in} \\ V_{in} \end{pmatrix} \tag{7}$$

In formula (7), δ_W is the retardation of the wave-plate, θ_W is the rotation angle of the fast-axis of the wave-plate. Therefore, the intensity of the light which passes through the polarimeter is expressed as follows;

$$I_{out} = \frac{1}{2} I_{in} + \frac{1}{4}\{(1+\cos\delta_W) + (1-\cos\delta_W)\cos 4\theta_W\} Q_{in} + \frac{1}{4}\{(1-\cos\delta_W)\sin 4\theta_W\} U_{in} + \frac{1}{2}\{\sin\delta_W \sin 2\theta_W\} V_{in} \tag{8}.$$

This formula means that we can calculate I_{in}, Q_{in}, U_{in}, V_{in} by measureing I_{out}, when we set δ_W or θ_W as at least four kinds of suitable values. In the SMART-magnetographs, we finally adopted wave-plates as linear retarders, whose δ_W are fixed and θ_W can be changed.

In the case of using a wave-plate, the following points are considered as factors by which a wave-plate affects the measurement accuracy.

a. Non-uniformity of retardation δ_W
b. Indefiniteness of retardation δ_W
c. Indefiniteness of rotation-angle θ_W

Therefore, we set the following specifications for δ_W and θ_W, so that the error due to them on each component of the Stokes parameters is suppressed within 0.1 % of intensity (I_{in}).

$$\mathbf{W}^{-1}(\delta_W + \Delta\delta_W)(\mathbf{W}(\delta_W)\,\mathbf{S_{in}}) - \mathbf{S_{in}} < \begin{pmatrix} 10^{-3} \\ 10^{-3} \\ 10^{-3} \\ 10^{-3} \end{pmatrix} \quad \Rightarrow \quad |\Delta\delta_W| < 0.2^\circ \tag{9}$$

$$\mathbf{W}^{-1}(\theta_W + \Delta\theta_W)(\mathbf{W}(\theta_W)\,\mathbf{S_{in}}) - \mathbf{S_{in}} < \begin{pmatrix} 10^{-3} \\ 10^{-3} \\ 10^{-3} \\ 10^{-3} \end{pmatrix} \quad \Rightarrow \quad |\Delta\theta_W| < 0.045^\circ \tag{10}$$

In these formulae, we use $\mathbf{S_{in}} = \begin{pmatrix} 1 \\ 0.20 \\ 0.20 \\ 0.30 \end{pmatrix}$ which is the value of the maximum scale of polarized light from the solar photosphere. The size of the measurement errors of the Stokes parameters using the polarimeter whose wave-plate has the maximum value of the above-mentioned acceptable errors depends on the number of rotation-angles of the wave-plate. For example, when we use four rotation-angles, the size of the measurement errors is expressed as follows;

maximum error of (9) $\Rightarrow$

$$\Delta\begin{pmatrix} I \\ Q \\ U \\ V \end{pmatrix} = \begin{pmatrix} 0 & \mp 1.7\times10^{-3} & \pm 5.9\times10^{-5} & 0 \\ 0 & \pm 1.7\times10^{-3} & 0 & 0 \\ 0 & 0 & \pm 1.7\times10^{-3} & 0 \\ 0 & 0 & 0 & \mp 2.6\times10^{-3} \end{pmatrix} \begin{pmatrix} I \\ Q \\ U \\ V \end{pmatrix} \tag{11}$$

maximum error of (10) $\Rightarrow$

$$\Delta\begin{pmatrix} I \\ Q \\ U \\ V \end{pmatrix} = \begin{pmatrix} 0 & \mp 2.0\times10^{-5} & \mp 6.0\times10^{-4} & \pm 4.2\times10^{-4} \\ 0 & -4.5\times10^{-6} & \pm 3.0\times10^{-3} & \pm 1.1\times10^{-3} \\ 0 & \mp 3.0\times10^{-3} & -4.6\times10^{-6} & \mp 3.7\times10^{-5} \\ 0 & 0 & 0 & -1.1\times10^{-6} \end{pmatrix} \begin{pmatrix} I \\ Q \\ U \\ V \end{pmatrix} \tag{12}$$

Next, we explain some further details of the actual quantities of the above-mentioned items a, b, and c.

a. Non-uniformity of retardation δ_W

Our wave-plates are made of quartz, and their thickness corresponds to 1st order. If we assume that the non-uniformity of retardation comes from only the non-uniformity of the thickness of the wave-plate (d_W), the acceptable error of thickness which fulfills the specification of (9) is $d_W = 94.31 \pm 0.04\ \mu$m. According to typical Japanese, Chinese and Australian makers, however, such a highly accurate polish is impossible or takes a huge amount of development expense. Therefore, finally, we decided to accept the following specification which was presented by a Japanese maker as a limit which can be manufactured.

$$\delta_W = 127.0 \pm 1.0° \qquad d_W = 94.31 \pm 0.2\ \mu m \tag{13}$$

After completing the two wave-plates for the two magnetographs, we measured the distributions of their retardations. As a result, we found the following averaged values and PV values (peak to valley) of the retardations.

Wave-plate 1: $\overline{\delta_W} = 127.98°, \quad PV = 1.81°$ (14)

Wave-plate 2: $\overline{\delta_W} = 127.68°, \quad PV = 1.78°$ (15)

Indeed we could confirm that the measured non-uniformities ($\pm$PV/2) fulfill the acceptable error of (13). However, they exceed the ideal specification shown in (9). This problem can lead to an enlargement of the measurement error of the magnetic field around the center of the sunspot where the sunlight has very large Stokes parameters. Therefore, we need to consider appropriate methods which can decrease the influence of this non-uniformity, such as increasing the number of rotation-angles of the wave-plate, for example, especially when we want to observe the very strong magnetic field in the center of a sunspot with high accuracy.

b. Indefiniteness of retardation δ_W

We can consider that there are two factors in indefiniteness of retardation. One is the measurement error itself of true retardation of a quartz wave-plate. The other is the unexpected temporal variation due to the change of the ambient temperature and so on.

Concerning the former, since the exact measurement of the retardation is very difficult, a comparatively large uncertainty is expected. For example, retardations of wave-plate 1, which were measured with three different kinds of instruments and methods, have an uncertainty in the following range at present.

$$125.065° < \delta_W < 127.98° \tag{16}$$

As concerns this indefiniteness, we intend to perform additional measurements and obtain the true value of the retardation.

On the other hand, concerning the temporal variation, we have a result from our theoretical simulations which show that the temperature dependence of the retardation of the 1st order wave-plate made of quartz is about –0.05° /℃. According to this result, we should suppress the fluctuation of the temperature of the wave-plate within $|\Delta T| < 4$ ℃ in order to realize the specification of (9). The SMART's structure is such that conditioned dry air can circulate through the space between the optics boxes and the wall. Moreover, electric heaters are installed near the wave-plates, so that they can control the ambient temperatures around the wave-plates locally. As a result, we have created an environment where the fluctuations of the ambient temperatures around the wave-plates are suppressed within 25± 1 ℃ throughout the year. Therefore, we can consider that the indefiniteness of the retardation due to the temperature-fluctuation is $|\Delta \delta_W| < 0.05°$ and this fulfills specification (9) sufficiently.

c. Indefiniteness of rotation-angle θ_W

We can consider that there are also two factors in the indefiniteness of the rotation-angle. One is the resolution of the encoder and the accuracy of the motor. The other is the installation accuracy of the zero-point of the wave-plate-axis compared with the standard axis of the polarizer.

Concerning the former, we must use encoders whose resolutions are better than 15-bit (angular resolution: 0.011°) in order to read the rotation-angle with a high resolution which is less than 1/3 of the acceptable error: 0.045° in formula (10). Actually, we selected ready-made encoders for direct-drive motors whose angular resolution is 0.00035° (1015808 p/rev). Moreover, we selected ready-made direct-drive motors whose uncertainty (repeating accuracy) is ±0.0014° . Therefore, the actual indefiniteness of our encoders and motors fulfills specification (10) sufficiently.

On the other hand, concerning the installation accuracy, we performed an examination measurement of the uncertainty of the wave-plate-axis compared with the standard polarizer-axis by setting one more temporary polarizer at the front of the wave-plate. As a result, this actual indefiniteness was

$$-0.042^\circ < \Delta\theta_W < +0.044^\circ \quad (17).$$

Therefore, this also fulfills the specification (10).

4.4 Simultaneous recording of two images of orthogonally polarized light by using Fabry-Perot channel

Though we use a Lyot filter in the T2-magnetograph, we use a Fabry-Perot filter in the T4-magnetograph. A Lyot filter has a polarizer which is installed just behind the entrance, so only the linear-polarized light whose oscillating direction accords with the polarizer's axis can pass through the Lyot filter. On the other hand, any linear-polarized light can pass through the Fabry-Perot filter. Therefore, in the T4-magnetograph, we installed a beam-splitting polarizer (prism) behind the Fabry-Perot filter and we observed two images of orthogonally polarized light simultaneously. This brings the effect of making various errors decrease, such as the influence of the non-uniformity of the retardation of the wave-plate, the influence of the seeing, and so on.

However, generally, a Fabry-Perot filter tends to easily have non-uniformities in the center wavelengths and FWHMs of the transmission profiles, because of restrictions of the polishing accuracy of the etalon made from $LiNbO_3$ etc., and the uniformity of the coating of the reflection materials. Therefore, it is considered to have a difficulty in obtaining highly accurate measurements of the polarization originating from solar magnetic fields. Especially when we want to suppress contaminations due to continuum light from sub-peaks to the main-peak intensity, we must make the thickness of the etalon very thin in order to make the intervals between every peak wide. Therefore, it becomes more difficult to attain high polishing accuracy and high uniformity in the shape of the etalon. Since measurement errors of 0.1 % of Q/I, U/I, V/I occur when there is a non-uniformity of only 1 % in the FWHM, the uniformity of the transmission profile of the filter is a very important element for the measurement of the polarization with high accuracy.

Therefore, in developing our filter for the T4-magnetograph, we decided to manufacture a tandem-type Fabry-Perot filter including two pieces of etalons whose thicknesses are sufficient to attain high polishing accuracy. Since these etalons have different appropriate thicknesses, the intervals between the peaks of each transmission profile are appropriately different. Therefore, when these two etalons are piled, all sub-peaks except for the main peaks are negated, and are offset. As a result, we can make the transmission profile, which has wide intervals between the main peaks, from comparatively thick etalons, which can not be made from only one etalon unless the thickness is polished very thin.

When we chose the combination of thickness of these two pieces of etalons, we simulated transmission profiles and their characteristics for many combinations. Then finally, we selected 300 μm+420 μm as the best thickness combination. This combination produces a transmission profile whose sensitivity to the change of the Stokes parameters corresponding to the magnetic field strength is the highest and whose sensitivity to the thickness error is the lowest among them (Table 2).

Table 2. Examples of combinations of thickness of tandem-type Fabry-Perot filter and their characteristics

Thickness	300 μm+420 μm	250 μm+350 μm	200 μm+280 μm
FWHM (Å)	0.101	0.152	0.122
Contamination from sub-peaks (%)	9.6	3.8	6.7
Ratio of V/I to 1G of longitudinal magnetic field	0.000154206	0.000130305	0.000100898
	(at the wavelength where V-profile, whose field strength is 500G, has the maximum value)		
Ratio of Q/I to 1G of transversal magnetic field	0.0000654626	0.0000592339	0.0000523406
	(at the wavelength where Q-profile, whose field strength is 500G, has the maximum value)		
Ratio of V/I to ±1nm of thickness error	0.00475094	0.00459986	0.00392003
	(at the wavelength where V-profile, whose field strength is 500G, has the maximum value)		
	corresponds to 30.8091G	corresponds to 35.3007G	corresponds to 38.8514G

The simulated transmission profile of this combination is shown in fig.4. The resolution of the measured magnetic field strength of this combination is 6 G to 0.1 % of V/I for longitudinal magnetic fields, and 15 G to 0.1 % of Q/I for transversal magnetic fields.
The T4-magnetograph, however, a the structure where two tilted flat mirrors, a relay lens unit, a telecentric lens and this tandem-type Fabry-Perot filter are included in the polarimeter between a wave-plate and a beam splitting polarizer. Therefore, the measurement of instrumental polarization due to their optical elements and the compensation for these effects are noted as important and difficult subjects for future investigation.

Fig.4. Transmission profile (simulation) of the tandem-type Fabry-Perot filter which we selected

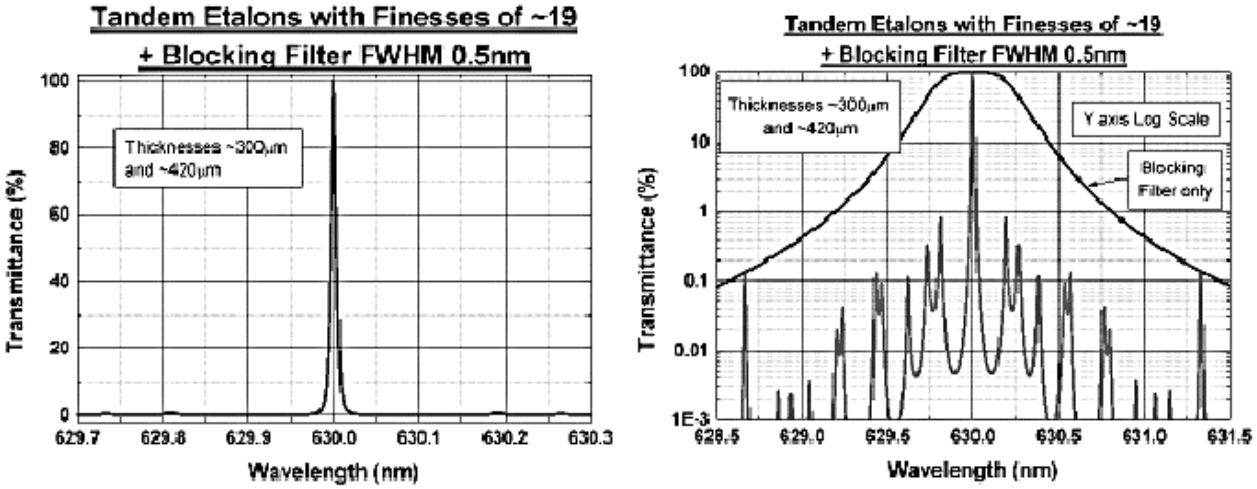

4.5 Observation of four wavelengths in an absorption line

In the case of the magnetograph which uses only one wavelength in the wing of an absorption line, influences of various errors are greatly reflected in the measurement accuracy of the polarizations, or the calculation accuracy of the vector magnetic fields. As the main origins of errors, the Doppler shift of the line due to solar atmospheric gas motion can be considered first. For example, about ±100 % error in the calculated magnetic field appears when the true given magnetic field strength is about 500 G and there is a Doppler velocity of 2 – 3 km/s. In addition, the measurement error of the polarization under the influence of errors of the center wavelengths of the Lyot filter and the Fabry-Perot filter and of the non-uniformity of their FWHMs etc. appears as a calculation error in the vector magnetic field directly.

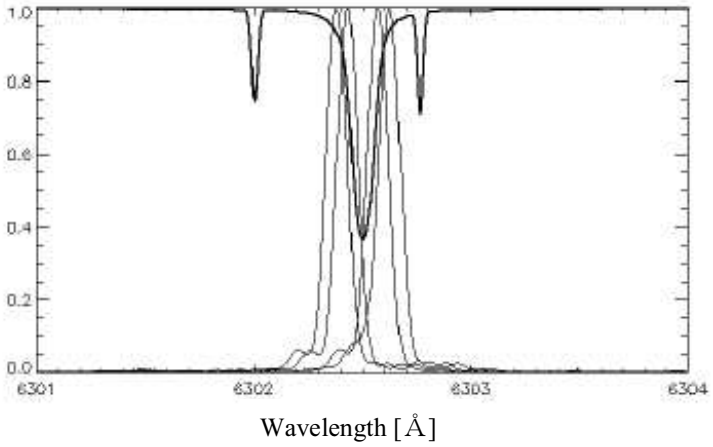

Fig. 5. Actual transmission profiles at 4 wavelengths of our Lyot filter and the solar absorption line

In order to suppress these various errors, multi-wavelength measurement is effective. We currently perform measurements with the four wavelengths; ±0.120, ± 0.070 Å from the line center (fig.5). Since the inversion method from the Stokes parameters measured at four wavelengths to the velocity field and the magnetic field is currently under investigation, we do not give further details here. One typical method is to prepare Look-Up-Table (LUT) which is calculated from the model atmosphere in advance. LUTs show the relationship between the velocity or the magnetic field and appropriate indices which can express the shapes of the Stokes profiles as uniquely as possible. Indices which we currently use are α and S_0 etc., which are defined as follows;

$$\alpha = \begin{cases} S_0/(-S_2) & when\ S_0 < 0 \\ S_0/S_1 & when\ S_0 > 0 \end{cases}$$
$$\begin{cases} S_0 = (F_1 + F_2) - (F_3 + F_4) \\ S_1 = F_1 - F_3 \\ S_2 = F_2 - F_4 \end{cases} \quad (18)$$

where F_1, F_2, F_3, F_4 are the values of the Stokes parameters at the four wavelengths respectively in order from the short wavelength side. The α can effectively reflect the amount of Doppler shift of the V-profile etc. comparatively independently of the magnetic field strength. And the value of S_0 effectively changes corresponding to the magnetic field strength. Indices similar to these are used also in the inversion process of SOHO/MDI (Y. Liu & A.A. Norton, 2001). Though they have used a different absorption line (Ni I 6767.784 Å, equivalent width: 83 mÅ, g=1.426) from our line, they reported that the calculation error of the magnetic field strength can be suppressed within 10 % in a wide range of magnetic field strengths (0 – 3000 G) by using data from four wavelengths, provided the Doppler velocity is less than 3 km/s.

4.6 Wavelength shift in the FOV due to the oblique incidence of the rays to the filters

When the incident angles of the rays which enter the narrow-band filters such as the Lyot filter and the Fabry-Perot filter are changed, the center wavelengths of the transmission profiles of the filters are also generally changed. Therefore, in the case of an optical system in which rays focusing to different positions on the focal plane have different incident angles at the filter, the obtained image reflects the different wavelengths in the FOV. If we perform the observation at multi-wavelengths, the amount of wavelength-shift can be detected and be compensated for with a certain accuracy. However, when this wavelength-shift becomes larger than a certain value, the calculation error of the magnetic field also becomes large suddenly, because the error in estimating the amount of wavelength-shift becomes large and the uniqueness of the relation between the observed Stokes parameters and the vector magnetic field begins to collapse.

As we described in section 4.5, if the amount of the Doppler shift exceeds 3km/s, in the case of Ni I 6767.784Å, the calculation error of the magnetic field strength becomes large and exceeds 10% suddenly. We use the absorption line: Fe I 6302.499 Å, equivalent width: 83 mÅ, g=2.5 in SMART-magnetographs. Since this line has the same width as the Ni line and has larger Zeemann splitting, we can consider that the sensitivity of this line to errors due to wavelength-shift is not larger than that of the Ni line. Therefore, we aimed at suppressing the total wavelength-shift, including both instrumental and solar origins, in solar quiet regions within 3 km/s, and set the specification that the wavelength-shift due to only incident rays oblique to the filters should be suppressed within 1 km/s. In other words, our specification is;

Wavelength-shift in the FOV due to the incident rays oblique to the filter: $|\Delta\lambda| < 0.021$Å (at 6302.5 Å) (19).

The Lyot filter (T2-magnetograph)

We use a Lyot filter whose FWHM is 0.125 Å. The maximum aperture of the Lyot filter with this FWHM is currently about ϕ32 mm. Since this aperture is too small to use the telecentric rays which cover the full solar disk, collimator rays enter into the Lyot filter in this magnetograph. In this case, however, the incident angles of the rays changes depending on the distance from the center of the FOV, according to the following equation.

$$\Delta\lambda = \frac{\mu}{4\omega^2\varepsilon} i^2 \lambda_0 = \frac{\mu}{4\omega^2\varepsilon}\left(\alpha\frac{D}{d}\right)^2 \lambda_0 \quad (20)$$

Where i: incident angle, ω=1.65437, ε=1.48459: refraction indices, $\mu = \omega - \varepsilon$=0.16978: birefringence index, λ_0: wavelength of incident ray, α: radius of FOV [rad], D: diameter of objective, d=3cm: diameter of pupil in the filter.

In order to realize specification (19), we can get the following condition for i and D from this equation.

$$i < 1.02^\circ, \quad D < 11 \text{ cm} \quad (21)$$

when α=1000 arcsec (=4.848x10^{-5} rad) and λ_0=6302.5 Å.

Then actually, we insert the ϕ10 cm diaphragm behind the second objective lens automatically in the full-disk mode of this magnetograph.

On the other hand, since the α of the partial-region mode is 354 arcsec, i is only 0.66° at the end of the FOV even if we do not use any diaphragm. Therefore the wavelength-shift is not a problem in this mode.

The Fabry-Perot filter (T4-magnetograph)

As we already mentioned in section 4.4, we use a tandem-type Fabry-Perot filter whose FWHM is 0.101 Å in the T4-magnetograph. The aperture of this filter is large: ϕ 60 mm and we observe only a partial-region with this magnetograph. Therefore we selected the telecentric optical system for this filter. As a result, all rays which focus to any position in the FOV have the same incident angle and the same F-number, so the difference of the wavelength-shift in the FOV does not occur.

4.7 Large format and highly sensitive CCD camera

When the exposure time of a CCD camera is comparatively short as in solar observations, the largest factor in the photometric errors is generally the photon noise. When we define S as the photon number, the photon noise is expressed $\sqrt{S}$. The ratio of the photon noise becomes lower as the photon number increases. The condition for the photon noise fulfilling the target photometric accuracy of (1) is as follows;

$$\frac{\sqrt{S}}{S} < 0.1\% \qquad (22).$$

In other words,

$$S > 1{,}000{,}000\ e^- \qquad (23).$$

Therefore, we need CCD chips whose "full-well" is larger than 1 Me^-. However, there were no chips which fulfill this specification among the ready-made chips whose pixel numbers are larger than 2Kx2K. Therefore, we selected the following CCD chip for the T2-magnetograph which has the largest full-well among them.

Pixel size: 14 μm, Pixel number: 2048x2048 pix^2, Full well: 200,000 e^-, Readout speed: 10 MHz/12bit (24)

On the other hand, the purpose of T4 is not only to be used as a magnetograph. Therefore, we chose the CCD chip which has a high performance in every characteristic rather than paying attention only to the full-well. Its characteristics are as follows;

Pixel size: 9 μm, Pixel number: 4096x4096 pix^2, Full well: 100,000 e^-, Readout speed: 5 MHz/12bit (25).

The ratio of the photon noise to the full-well of the CCD (24) is 0.22 %, and that of the CCD (25) is 0.32 %, which exceeds our specified photometrical error. Therefore, we need to suppress the noise ratio further by some method such as multi-wavelength observations, as we mentioned in section 4.5.

On the other hand, the size of the readout noise of the CCD (24) is about 35 – 40 e^- (= 0.018 – 0.020 %), that of the CCD (25) is about 35 e^- (= 0.035 %). Therefore, these noises are not considered important for influencing the accuracies.

4.8 High speed data transfer interface from CCD to PC

The data transfer interface and its speed are important factors which directly influence the temporal resolution. In the T2-magnetograph, since we use the above-mentioned CCD (24), the size of the data is 8 MB/frame and the readout speed is 10 Mpix/sec (= 20 MB/sec). In the T4-magnetograph including the CCD (25), the size of the data is 32 MB/frame and the readout speed is 5 Mpix/sec (= 10 MB/sec). Therefore, we requested a data transfer interface whose speed is high enough (> 20 MB/sec) to obtain an effective readout speed for the CCD. Therefore, finally, we chose the USB2.0 interface this time. Since the ideal transfer speed of the USB2.0 is 480 Mbit/sec (= 60 MB/sec), this value fulfills the above-mentioned required value sufficiently. The required time for image transfer is considered to be 0.4 sec/frame (= 6.4 sec/series) for the T2-magnetograph and 3.2 sec/frame (= 38 sec/series) for the T4-magnetograph under ideal conditions. However, the actual transfer speed with the USB2.0 has an indefiniteness depending on the environment and time zones etc. because of delays for safety securements by driver softwares, such as the re-trying process to deal with transfer failures due to noise environments.

Anyway, the required time for only image transfer in 1 series of the T2-magnetograph is sufficiently shorter than the target temporal resolution of (2). On the other hand, that of the T4-magnetograph already exceeds the target temporal resolution. Therefore, we consider that we will choose a suitable method according to the scientific purpose, comparing the merit of giving priority to the pixel-resolution with the merit of giving priority to the temporal resolution (in other words, data size will be reduced by binning) in the process of future operations of the T4-magnetograph.

5. SUMMARY AND FUTURE SUBJECTS

We have performed various tests and advances while developing SMART-magnetographs as we introduced in section 4 in order to obtain highly accurate measurements of the polarization components originating from the solar magnetic field. Though there are many items with which our target specifications are fulfilled, there are several items in which our target accuracies are not fulfilled or whose actual errors have not been measured. After measuring the actual accuracies

of all the remaining items and estimating the size of the errors of the calculated vector magnetic field, we intend to report the final actual accuracies of the SMART-magnetographs at another opportunity.
We describe main tasks which should be completed below.

- Measurements of the instrumental polarizations before the polarimeters, in other words, Muller matrices of wedge-shaped pre-filters and objective lens units
- Accumulation of measurement data of the absolute value of the retardation of the quartz wave-plate and actual measurements of the temperature dependences of the retardations of the wave-plates
- Measurements of the actual transmission profiles of the Lyot filter and of the Fabry-Perot filter and examination of their uniformities and stabilities
- Measurement of the Muller matrices of the optical elements in the polarimeter of the T4-magnetograph
- Determination of an inversion method from the Stokes parameters at four wavelengths to velocity and magnetic fields, and estimates of the errors of the magnetic fields calculated with the inversion method
- Inspection of the final temporal resolution in each observation mode
- Examination of the typical size of the apparent polarization components due to seeing, and compensation for it by software

We will clarify these issues, and continue aiming to supply reliable highly accurate data of the vector magnetic field.
Finally, we display an example of each component of the "vector magnetogram" obtained on October 30, 2003 with the full-disk mode of the T2-magnetograph in fig. 6, though they are not yet compensated for the instrumental polarization nor calculated with the final inversion method.

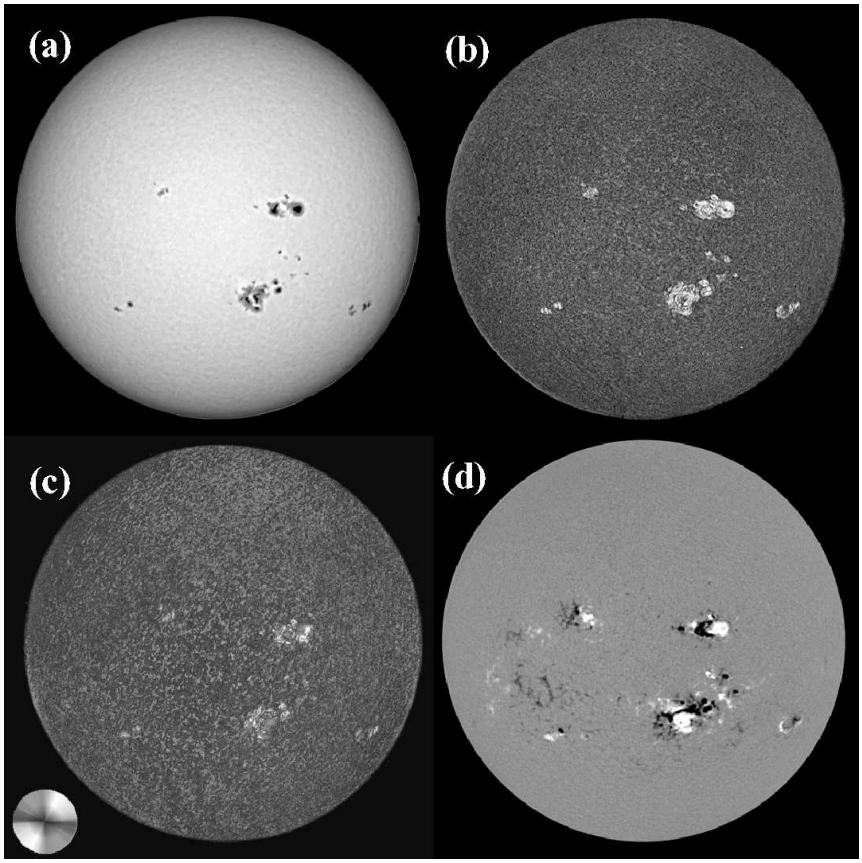

Fig.6. Vector magnetogram obtained by T2-magnetograph of the SMART on October 30, 2003.
a: Intensity map, b: $(Q^2+U^2)^{1/4}$-map, c: azimuth angle map, d: V-map

REFERENCES

1. K. Kusano, T. Maeshiro, T. Yokoyama and T. Sakurai, ApJ, 577, 501, 2002
2. H. Holweger and E. A. Muller, Solar Physics 39, 19, 1974
3. Y. Liu and A. A. Norton, SOI-Technical Note 01-144, 2001